Journal of Applied Polymer Science

Oxidation of γ-Irradiated Microbial Cellulose Results in Bioresorbable, Highly Conformable Biomaterial

Wojciech Czaja, Dmytro Kyryliouk, C. Alex DePaula, Douglas D. Buechter
DePuy Synthes Biomaterials, 1230 Wilson Drive, West Chester, Pennsylvania 19380
Correspondence to: W. Czaja (E-mail: czaja.wojciech@synthes.com)

ABSTRACT: Conformability to tissues and adequate mechanical strength are clinically useful properties of resorbable biomaterials used in soft tissue repair. Microbially derived cellulose is attractive as a high strength, highly conformable, and biocompatible material for tissue repair, but is not naturally resorbable. Here we show that controlled oxidation of microbial cellulose sheets that have been pre-irradiated with γ-radiation results in a resorbable and fully conformable membrane that can be rapidly rehydrated in aqueous fluids. *In vitro* studies showed that degradation of the resorbable membranes occurs in two major phases: (1) initial rapid degradation of about 70–80% of the entire sample followed by (2) slower degradation of an additional 5–10% which eventually levels off leaving a small amount of nonresorbable material. *In vivo*, prototype materials showed marked degradation at all time points, with the most rapid degradation occurring in the first 2–4 weeks. © 2013 Wiley Periodicals, Inc. J. Appl. Polym. Sci. **2014**, *131*, 39995.

KEYWORDS: biomaterials; biosynthesis of polymers; cellulose and other wood products; biocompatibility; bioengineering

Received 15 July 2013; accepted 23 September 2013
DOI: 10.1002/app.39995

INTRODUCTION

Cellulose of various origins has been proven to be a versatile biomaterial, particularly well suited for the creation of unique biomedical devices. Synthesized by just about every type of plant and a select number of bacteria, it is an all-natural, renewable, biocompatible, and biodegradable polymer used in a wide variety of applications ranging from paper products, electronics, drug coatings and bandages to food desserts and electronic paper.[1–4]

Cellulose produced in bacteria has long been recognized as a novel biomaterial with potential for temporary wound coverage, for treatment of chronic wounds and burns, as a scaffold for tissue growth, synthetic blood vessels, as well as many other biomedical applications.[2,5–9] A particularly unique type of cellulose synthesized by *Acetobacter xylinum* (reclassified as *Gluconacetobacter,* and more recently as *Komagataeibacter*) is characterized by a highly crystalline three-dimensional network consisting of pure cellulose nanofibers that is stabilized by inter- and intrahydrogen bonds.[10] Such a fibrilar network displays high strength, water-holding capacity, and conformability to irregular surfaces making it particularly well suited for soft tissue repair and reinforcement.

Native plant or bacterial cellulose cannot be degraded in humans because of the lack of enzymatic machinery capable of breaking down the β(1-4) glucose linkages. Resorbability of cellulose can be, however, achieved through oxidation of the glucose units using various chemicals, including metaperiodate, hypochlorite, dichromate, or nitrogen dioxide.[11] Oxidized plant cellulose has been successfully used as a resorbable hemostat since 1949. For this application it is oxidized most effectively through the use of nitrogen dioxide gas vapor that produces material with high carboxyl content.[11] However, sodium metaperiodate has proven to be more selective when oxidizing highly crystalline celluloses with minimal side reactivity.[12] Metaperiodate-mediated oxidation of cellulose has been studied extensively on plant cellulose and to some extent bacterially derived cellulose.[11,13–18] Li et al. prepared a degradable 3-D nano-network from bacterial cellulose by periodate oxidation and tested it *in vitro* as a potential tissue engineering scaffold.[19] Periodate cleaves the C2-C3 bond in the glucopyranose ring and the resulting hydroxyl groups are subsequently further oxidized to dialdehyde groups. Dialdehyde-containing plant cellulose is believed to biodegrade by hydrolysis under physiological conditions to 2,4-dihydroxybutyric acid and glycolic acid.[14] As far as we know, this is the first study describing the *in vivo* degradation and resorption of periodate-oxidized microbial cellulose (OMC).

Other interesting approaches to resorbable cellulose have been recently described but with very little or no *in vivo* biocompatibility and resorption data. Yadav et al. reported a metabolic engineering approach to the redesign of cellular metabolic pathways to introduce N-acetyl-glucosamine residues into cellulose chains during *de novo* synthesis in *A. xylinum*.[20] The novel chimeric

polymer showed reduced crystallinity and *in vivo* susceptibility to human lysozyme. Hu and Catchmark reported development of resorbable microbial cellulose by incorporating cellulase enzymes into its nanostructure.[21] A freeze-dried polymer was tested mechanically but no detailed quantitative information on *in vitro* and *in vivo* degradation profiles was provided.

It is known that the oxidation process can significantly alter the structure of cellulose.[11] With microbial cellulose it may result in significant disruption of its unique, medically desirable properties, i.e. high tensile strength and conformability. This is particularly notable for soft tissue applications where the material often needs to readily conform to the various contours of the body, have adequate strength for tissue support and reinforcement and allow easy handling, but also to be resorbable over a time frame that is compatible with healing of the particular anatomical site. Consequently new and improved methods for oxidizing cellulose and achieving these properties are needed. Here we describe a controlled oxidation process of γ-irradiated microbial cellulose that results in a resorbable, porous, and yet strong and conformable biomaterial (2,3-dialdehydecellulose) in the form of a dry patch. *In vitro* and *in vivo* degradation, mechanical testing and microscopic observations are presented and discussed along with the proposed mechanism of *in vivo* resorption.

EXPERIMENTAL

Microorganism and Culture Conditions

A proprietary *A. xylinum* strain from the collection of DePuy Synthes was used in this study. Bacteria were grown in a culture medium with sucrose as the main carbon source and corn steep liquor as the main nitrogen source. The bacterial cells for the inoculum were cultured in Erlenmeyer flasks filled with media for a period of 2–3 days at 30 ± 2°C. These growth media with cellulosic pellicles were then gently stirred and used as inoculum for large-scale fermentation in tray reactors. The trays were incubated in static conditions at 30 ± 2°C for a period of 5 days until a uniform pellicle formed on the surface. Pellicles were harvested and purified by washing with 3% aqueous NaOH and bleached with 0.25% H_2O_2. Purification was completed by soaking pellicles in distilled water to achieve a neutral pH. Finally the pellicles were mechanically pressed to 1 mm thickness using Carver press at 1000 psi, and γ-irradiated at the range of 22.5–29 kGy by Sterigenics.

Sodium Periodate Oxidation

Purified and γ-irradiated cellulose sheets were incubated in the dark on a rotary shaker in an excess of aqueous solution of 0.3*M* $NaIO_4$ for 1–6 hours at 40°C (molar ratio $NaIO_4$ / glucopyranose unit = 120). The oxidation reaction was stopped by thoroughly washing samples in DI water for 3–4 hours.

Determination of Dialdehyde Content (Oxidation Degree)

Aldehyde content in the oxidized cellulose membranes was determined by the Canizzaro method.[22] Briefly, oxidized samples were reacted with 10 mL of 0.05*M* NaOH at 70°C for 15–25 minutes with stirring. The resulting suspension was cooled to room temperature and 10 mL of 0.05*M* HCl added. The excess acid was titrated with 0.01*M* NaOH using phenolphthalein as an indicator. The following formula was used to calculate dialdehyde content:

$$\%\,\text{Oxidation/Dialdehyde group} = (\{[V_1 - V_2)\text{N}162]/(\text{M})\} \times 100)/2$$

where V_1 is the amount (L) of NaOH used to titrate solution, V_2 the amount (L) of NaOH used to titrate solution with no cellulose, N the concentration of NaOH used for titration, and M the weight (g) of cellulose sample.

Supercritical CO_2 (sCO_2) Drying

Oxidized cellulose sheets were extracted with ethanol by conducting a stepwise extraction: 30%, 50%, 90% (v/v) and absolute ethanol for 3 hours at each percentage. Samples were then dried using a Speed SFE supercritical CO_2 extraction system (Applied Separations, Allentown, PA).

Mechanical Testing and Conformability

OMC samples were tested for ball burst strength using either an Instron mechanical testing machine (Model 5500R; Instron, Norwood, MA) or a manual burst tester, custom made by Synthes, USA, and calibrated at 11.4 kg (25 lbs). Conformability was evaluated by rehydrating sCO_2-dried samples in simulated body fluid (SBF; pH = 7.4) and visually assessing the ability to conform to irregularities on the surface of the Cranial Pulsation Model (Synthes, USA).[23] A fully conformable sample was defined as rehydration within 10 seconds and complete adherence to the surface of the dura model.

Sample Density (Cellulose Content)

Samples with a known surface area were air-dried to constant weight at 55°C overnight. Cellulose content was calculated by dividing the weight of the dried sample by its surface area, yielding units of g/cm^2.

SEM

Oxidized, sCO_2-dried samples were sputter coated with gold (Denton Vacuum, Desk IV, Moorestown, NJ, USA). A Hitachi S-570 field emission scanning electron microscope operating at 20 kV was used for examinations of the samples.

FTIR Spectroscopy

Oxidized, sCO_2-dried samples were placed across the FTIR stage and run using DATR spectroscopy. Spectra were recorded on Thermo Nicolet Nexus 470 spectrometer with accumulation of 64 scans at a resolution of 1 cm^{-1} in the range from 4000 to 400 cm^{-1}.

XRD

X-ray diffraction (XRD) spectra were recorded using Ni filtered Cu-Kα radiation produced by the PANalytical XRD System. Scans were performed over the 4–90° 2θ range, but analyzed from 4° to 40° 2θ range. The data were analyzed with the HighScore Plus XRD software. Percent crystallinity was calculated using the following equation:

$$\text{CrI} = 100[(I_{002} - I_{\text{Amorph}})/I_{002}],$$

where CrI is the degree of crystallinity, I_{002} is the maximum intensity of the (002) lattice diffraction (22° 2θ), and I_{Amorph} is the intensity diffraction at 18° 2θ.[24]

Determination of Degree of Polymerization

The wet cellulose samples were homogenized in food processor with 60–70 mL of pure water for 60–90 seconds, resulting in slurries of very small fibrous particles. The slurries were then vacuum filtered using nylon membranes to remove excess water. The wet cellulose samples were then transferred to Whatman Vecta-Spin centrifuge filters, which contained 10-μm polypropylene mesh filters. The water was centrifuged off and replaced with HPLC grade methanol and soaked overnight. The following day the methanol was spun off, and an additional 3-hour soak with fresh methanol was performed, followed by a 20-minute centrifugation. The solvent exchange process was then repeated using dried N,N-dimethylacetamide (DMAc) for three exchanges with soak times of 75 minutes, overnight, and 30 minutes, with 20 minutes centrifugation after each soak. The DMAc-wet samples were then transferred into a solution of 8% lithium chloride in DMAc and stirred for 72 hours at room temperature. The diluted solutions were stored at approximately 4°C for an additional day before being filtered through 0.45-μm pore size PTFE syringe filters into GPC autosampler vials. The analysis was conducted by Polymer Solutions (Blacksburg, VA, USA).

Pyrogenicity Testing

Extracts of samples were tested for bacterial endotoxins using the kinetic-chromogenic LAL test.[25]

In Vitro Degradation Studies

Both real-time and accelerated degradation studies were conducted. Weighed samples (approximately 1 × 1 cm squares) were placed in sterile 50 mL centrifuge conical tubes filled with 20 mL of SBF (pH=7.4) and kept in static conditions at 37°C or 55°C for a period of time between 7 and 14 days.[26] SBF in each tube was changed after 5 days by centrifuging samples, decanting the SBF and replacing with fresh SBF. Samples were analyzed for degradation at 1, 2, 3, 4, 7, and 14 days. At each time point, tubes were centrifuged, the supernatant was decanted and the pellet washed twice with DI water. The pellet was then dried at 60°C to a constant weight. The percent of degradation was calculated as the difference between the dry pellet weight and original sample weight.

In Vivo Studies

Sixteen male New Zealand White rabbits were assigned to one of four groups of four animals each. Four samples of OMC and two control samples (Control Devices 1 and 2, commercially available crosslinked bovine tendon collagen (CD1, DuraGen Plus™, Integra LifeSciences, NJ, USA) and non-OMC (CD2), respectively) were implanted into separate subcutaneous pockets on the rabbit's back (three on each side of the dorsal midline). Cellulose samples had the following oxidation degrees: 50% (TD50), 55% (TD55), 84% (TD84), and 94% (TD94). The location of each implant in each rabbit was randomized according to a predetermined implantation matrix. After each test device or control device was implanted, a pair of 4-0 Prolene nonresorbable sutures were used to tie down the implant to the underlying subcutaneous tissue in order to minimize implant migration after implantation.

Four rabbits were euthanized and subjected to necropsy at each of the four different time points: 2 weeks, 4 weeks, 12 weeks, or 26 weeks after implantation surgery. Necropsy was limited to gross observations of the implantation sites and peri-implant tissues, with limited tissue collection (collection from the operative sites of the implant surrounded by peri-implant tissues). The degradation of the implant at each site was visually scored as follows:

0=same as when implanted
1=slight fragmentation,
2=moderate fragmentation,
3=severe fragmentation,
4=not able to score (i.e. no material present).

Tissues collected from the implant sites were fixed in 10% neutral buffered formalin and sections through the approximate center of the implant site were taken and embedded in paraffin. Hematoxylin and eosin (H&E) staining and Schiff staining (PAS) were performed. All slides were examined and reviewed by two board certified veterinary pathologists. Evaluation of the tissue response to the test and control devices, including scoring the degree of vascularization, fibrosis, and immune response, of the test and control devices and scoring the degree of irritation of the tissue at the implant site were performed, following the ISO 10993-6.[27] The total irritancy score was calculated from the sum of the overall inflammatory response (times two), vascularity, and fibrosis pathology scores. The total irritancy score was used to determine the following severity grade for irritant status:

–Nonirritant (0.0–2.9)
–Slight irritant (3.0–8.9)
–Moderate irritant (9.0–15.0)
–Severe irritant (>15.0)

Average ranked irritation scores were calculated for each test device at each time point by subtracting the average irritancy score for either CD1 or CD2 from each test device, and were based upon the guidelines as described in ISO 10993-6 (Annex E).[27] The surgeries were conducted at Preclinical Surgical Services (Winston-Salem, NC) and complied with the Institutional Animal Care and Use Committee of Wake Forest University. The pathology was performed at Alizee Pathology (Thurmont, MD).

RESULTS AND DISCUSSION

Oxidation Reaction

Periodate can oxidize highly crystalline regions of cellulose but it often results in formation of nonhomogenously oxidized structures, where dialdehyde groups are formed in spaced, band-like domains along the microfibrils.[13] Our work demonstrated that native microbial cellulose undergoes significant structural changes when oxidized with periodate. Careful control of reaction conditions during oxidation with metaperiodate is a key element to achieve a stable product with desirable

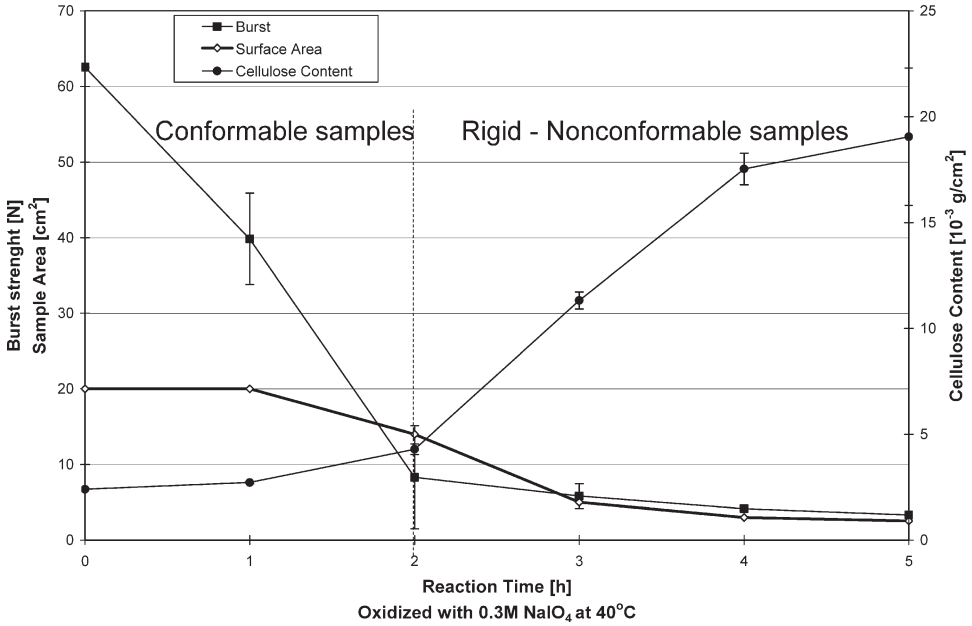

Figure 1. The influence of oxidation reaction time on physical and mechanical properties of nonradiated cellulose membrane.

physical and mechanical properties. In order to achieve a high oxidation degree (which directly translates to high degradation rate) without causing extensive depolymerization that could adversely affect physical and mechanical properties, certain key parameters of the reaction (i.e. temperature, periodate concentration, molar ratio of substrate to oxidant) have to be optimized. In our work, we chose to fix the base conditions of a reaction temperature of 40°C and periodate concentration of 0.3*M* because they resulted in moderate oxidation in experimentally manageable timeframes (data not shown). In addition, the reaction was conducted in the dark to minimize spontaneous decomposition of periodate that may have resulted in formation of free radicals, causing a significant random depolymerization of glucan chains.

Starting with these base conditions, we explored the effect of reaction time on the properties of the OMC material. Figure 1 shows the effect of reaction time on several important features of native (nonirradiated) microbial cellulose. At reaction times of 2 hours or more, a significant decrease in surface area was accompanied by an increased cellulose density of the membrane. Oxidation also resulted in a more compact structure with fibrils being stacked together rather than more dispersed as in native microbial cellulose (Figure 2A and B). In addition, mechanical testing showed that oxidation decreases the burst strength of the cellulose membrane, which further progresses with increasing reaction time (Figure 1). The overall handling of the final oxidation product in its dry form was also influenced by the reaction time. Our observations showed that the product becomes very rigid and brittle once the reaction proceeds beyond 2 hours. The product had no conformability even when extended rehydration times were applied. The high molecular weight and high crystallinity of microbial cellulose seems to be the major reasons for the vast structural changes of the cellulose upon oxidation. Others have also reported similar changes when oxidizing plant-originated cellulose.[18,28]

In addition to control of the variables discussed above, we found that exposure of cellulose membranes to γ-irradiation prior to oxidation resulted in improved handling properties. Figure 3 shows the influence of oxidation reaction time on key properties of the pre-irradiated cellulose membrane. While surface area decreases similarly to oxidized, nonirradiated samples and a comparable increase of cellulose density occurs, the

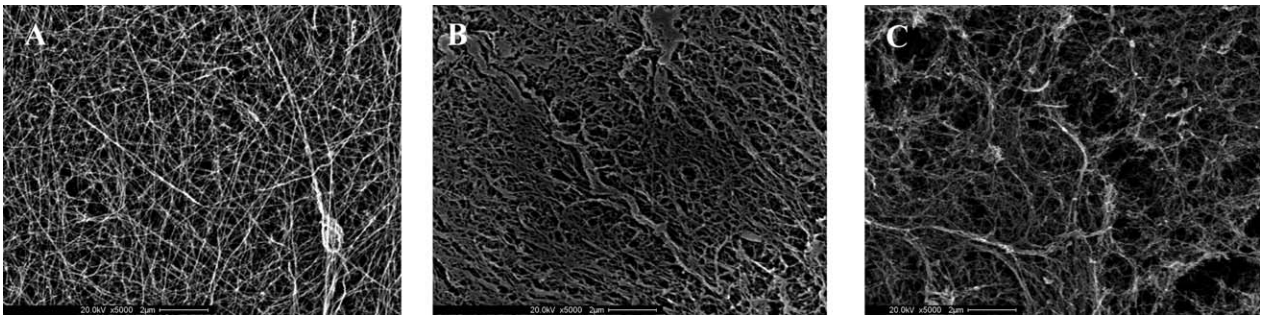

Figure 2. SEM images of: (A) native cellulose, (B) nonradiated, oxidized cellulose, and (C) pre-irradiated, oxidized cellulose.

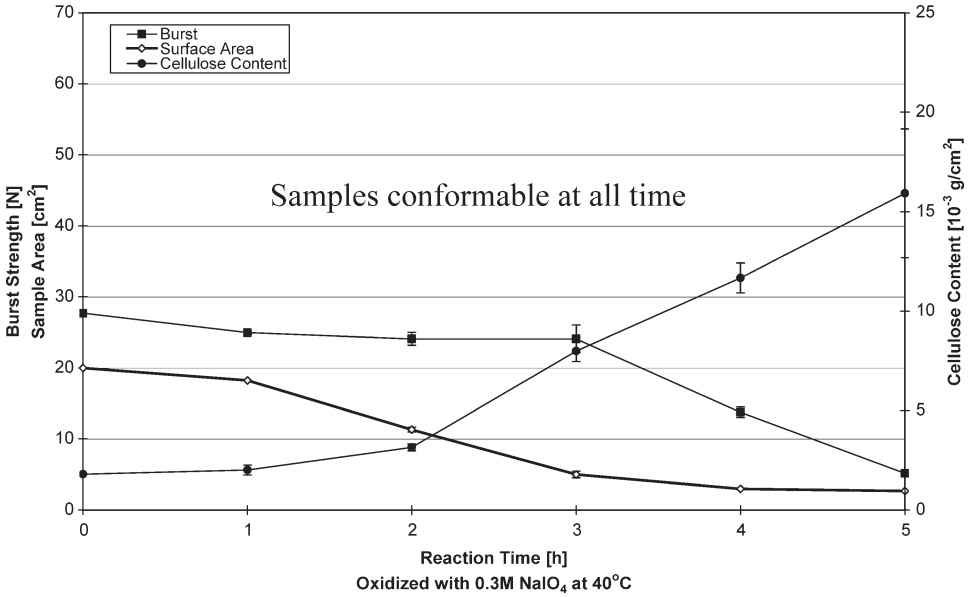

Figure 3. The influence of oxidation reaction time on physical and mechanical properties of γ-radiated cellulose membrane.

samples remained conformable regardless of the oxidation time (up to 5 hours). In addition, although pre-irradiated cellulose has less initial strength compared to nonirradiated, oxidation did not further decrease the strength out to 3-hour reaction times. SEM images (Figure 2) revealed that the structure of pre-irradiated oxidized material was disrupted and more chaotic than native cellulose with smaller, highly dispersed microfibrils and regions of heterogenicity. These images confirmed that the regions with densely packed fibrilar structures, typical for oxidized cellulose, were almost absent in the case of pre-irradiated oxidized cellulose. As a result, the conformability of the oxidized product was highly improved upon pre-irradiation. The collapsed nature of the oxidized cellulose in comparison with more open structure of pre-irradiated oxidized cellulose may suggest that long-chain cellulose was converted into short-chain crosslinked cellulose as a result of irradiation. The effect of increased intramolecular and intermolecular hydrogen bonding in cellulose upon γ-irradiation has been already described.[29,30]

Irradiation of cellulose has been previously shown to be an efficient method to reduce molecular weight and crystallinity of cellulose and also significantly increase its available surface area.[31,32] In our process, irradiation most likely resulted in induced scission of the long glucan chains and formation of lower molecular weight products. These changes in the physical properties of microbial cellulose made it more susceptible to oxidation with periodate, resulting in more limited gross structural changes.

Figure 4 shows X-ray diffractograms profiles of native and oxidized cellulose samples. It appears that the well-defined pattern of cellulose I for native bacterial cellulose diminishes for oxidized cellulose and changes even more significantly for pre-irradiated-oxidized cellulose. The presence of the diffuse peaks at the $(1\bar{1}0)$ plane for the irradiated OMC's suggest changes in hydrogen bonding resulting from the radiation and oxidation of cellulose [Figure 4(c)]. While these X-ray profiles suggest that the overall crystallinity of cellulose decreases during the course of oxidation, crystallinity index values also indicate that parts of crystalline cellulose were already disrupted by irradiation process prior to oxidation (Table I). The crystallinity indexes of the samples shown in Table I confirm a gradual decrease of the crystallinity for samples that are radiated and further oxidized. Interestingly, the difference between the crystallinity index of the nonradiated oxidized cellulose and radiated oxidized cellulose is relatively small. This may suggest that pre-irradiation creates a more open and accessible cellulose structure, resulting in more uniform oxidation, whereas the overall loss of crystallinity is more significantly affected by oxidation reaction conditions.

The FTIR spectra of native and oxidized cellulose (radiated and nonradiated) are shown in Figure 5. The characteristic bands of dialdehyde cellulose, in the region of 1740 and 880 cm^{-1} are visible for both oxidized cellulose samples in comparison with native cellulose. These bands are due to the carbonyl group stretch (1740 cm^{-1}) and to hemiacetal bonds between newly formed aldehyde groups and adjacent hydroxyl groups (880 cm^{-1}).[13,28,33,34] The slightly smaller band at 1740 cm^{-1} for radiated OMC in comparison with nonradiated-oxidized cellulose may suggest that: (a) more significant depolymerization occurred during oxidation of irradiated samples, or/and (b) more extensive formation of hemiacetal structures was triggered during oxidation of irradiated samples (slightly larger band at 880 cm^{-1}).

Figure 6 shows the degree of OMC membranes and provides further evidence that initial irradiation of cellulose changes the overall rate of oxidation. The reaction proceeds faster for radiated samples, especially within the first 2 hours. This might be caused by shorter glucan chains being oxidized more readily because of the disrupted crystallinity of irradiated cellulose. In other words, radiation pretreatment of high molecular weight cellulose changes its physicochemical properties and enhances its reactivity.[31] It was reported by others, for example, that

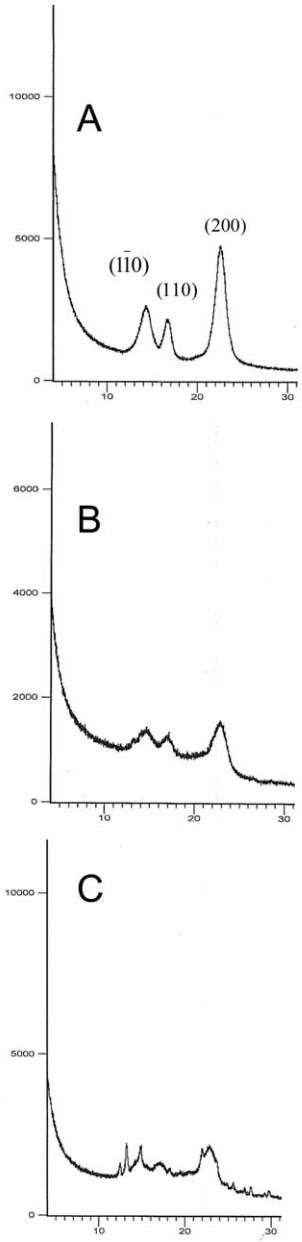

Figure 4. X-ray diffractograms of native and oxidized cellulose: (A) nonradiated native cellulose, (B) nonradiated oxidized cellulose, and (C) radiated oxidized cellulose.

irradiation strongly affects the rate of cellulose nitration and degree of substitution.[31] Irradiation of plant raw materials decreases the content of semi-hydrolysis-resistant polysaccharides and increases the content of hydrolysable ones because of

Table I. Crystallinity Index for Cellulose Samples

Cellulose sample	CrI [%]
Native nonradiated	81.9
Native radiated	72.0
Nonradiated oxidized	36.3
Radiated oxidized	35.3

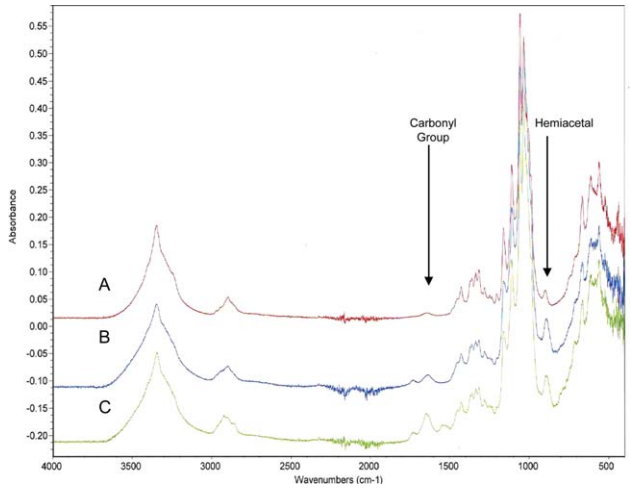

Figure 5. FTIR spectra of: (A) native cellulose, (B) irradiated-oxidized cellulose, and (C) nonradiated-oxidized cellulose. [Color figure can be viewed in the online issue, which is available at wileyonlinelibrary.com.]

radiation induced degradation of polysaccharides.[31] While both oxidized samples eventually reach the same degree of oxidation the conformability of samples is drastically different (Figure 7).

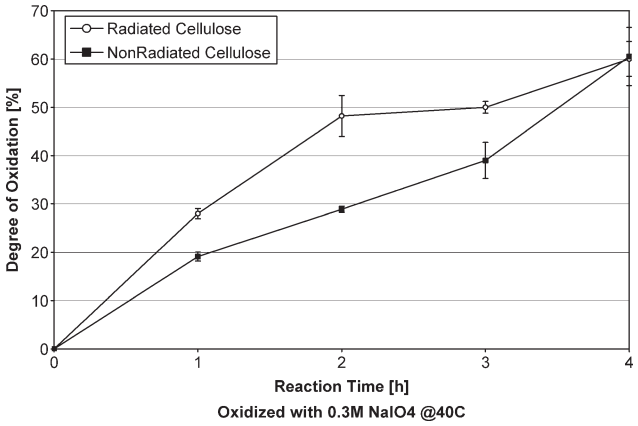

Figure 6. Degree of oxidation profile for radiated and nonradiated cellulose oxidized for various periods of time.

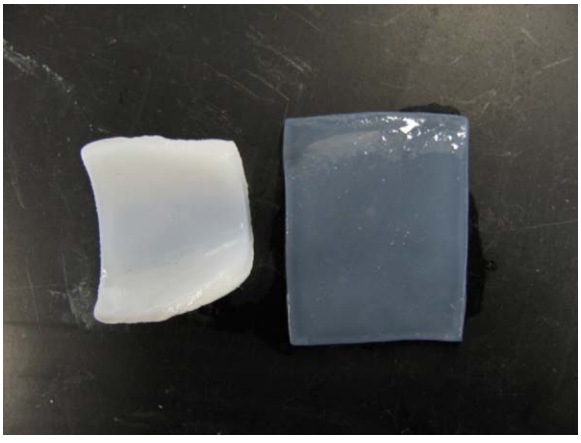

Figure 7. Photographs of rehydrated (left) oxidized nonradiated and (right) oxidized, pre-irradiated cellulose samples. [Color figure can be viewed in the online issue, which is available at wileyonlinelibrary.com.]

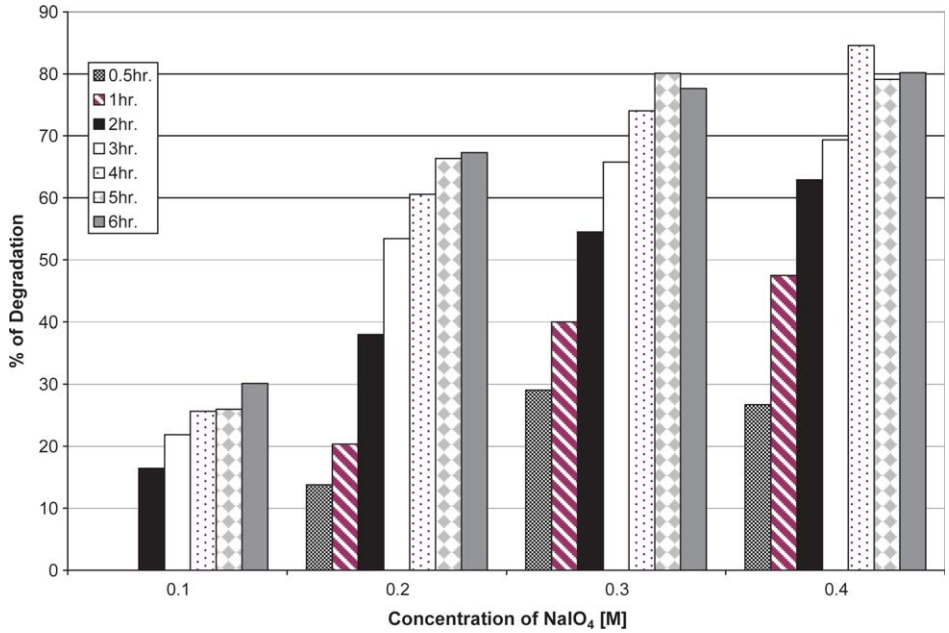

Figure 8. Degradation extent (SBF; pH=7.4, 55°C, 7 days) of radiated cellulose oxidized at 40°C at various times and different periodate concentrations. [Color figure can be viewed in the online issue, which is available at wileyonlinelibrary.com.]

In Vitro Degradation

Oxidized plant cellulose undergoes hydrolysis when exposed to alkaline conditions.[15] According to Stilwell *et al.* the degradation process appears to be controlled by the carbonyl content arising from the oxidation of the hydroxyl groups at C-2 and C-3 to carbonyl moieties.[11] These moieties introduce an alkali labile linkage rendering the adjacent glucosidic groups sensitive to alkali-mediated β-elimination.[11] Once the degradation process is initiated it continues along the glucan chain.[11] The hydrolytic scission results in formation of glycolic acid and 2,4-dihydroxybutyric acid. Both of these degradation products are known to be biocompatible and biodegradable and can be metabolized by the body.[15,16]

Figure 8 shows the extent of *in vitro* degradation after 7 days of irradiated cellulose, oxidized at different periodate concentrations and for different reaction times. For all conditions tested, a progressive loss of sample mass was observed during the 7 day period, and the samples became progressively softer and more gel-like with a high degree of transparency. Depending on the oxidation conditions used, a degradation range of 30–85% was achieved during 7 days incubation time. The results show that degradation rate is highly dependent on oxidation degree, which can be controlled by periodate concentration and reaction time.

A conformable and mechanically stable biomaterial with a defined degradation rate can be successfully prepared by starting

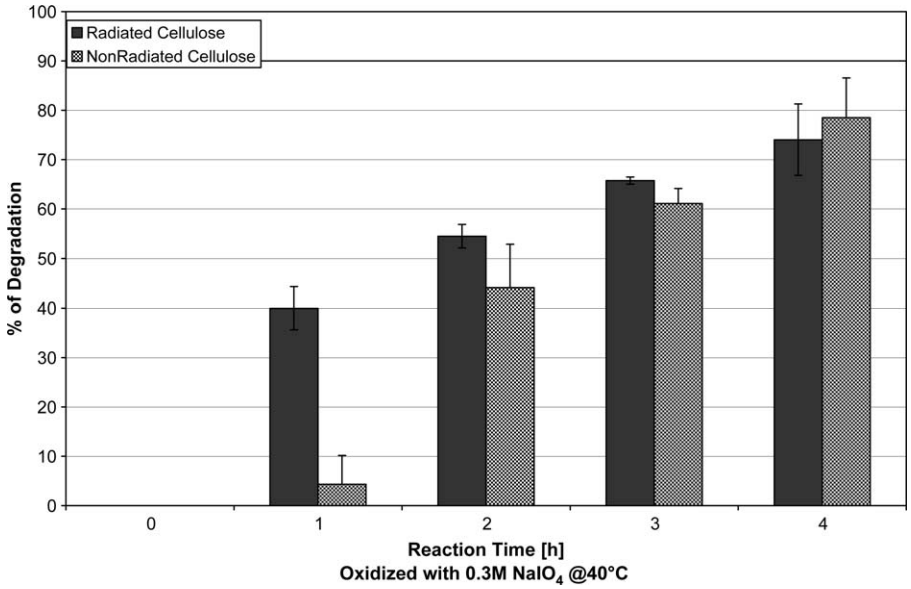

Figure 9. Degradation extent at 14 days incubation at SBF for radiated and nonradiated cellulose oxidized for various periods of time.

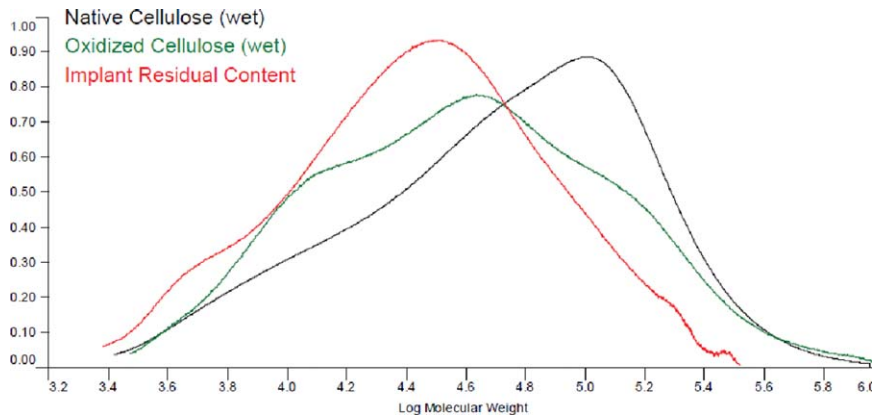

Figure 10. Overlay of the differential molecular weight distribution plots for the indicated samples. [Color figure can be viewed in the online issue, which is available at wileyonlinelibrary.com.]

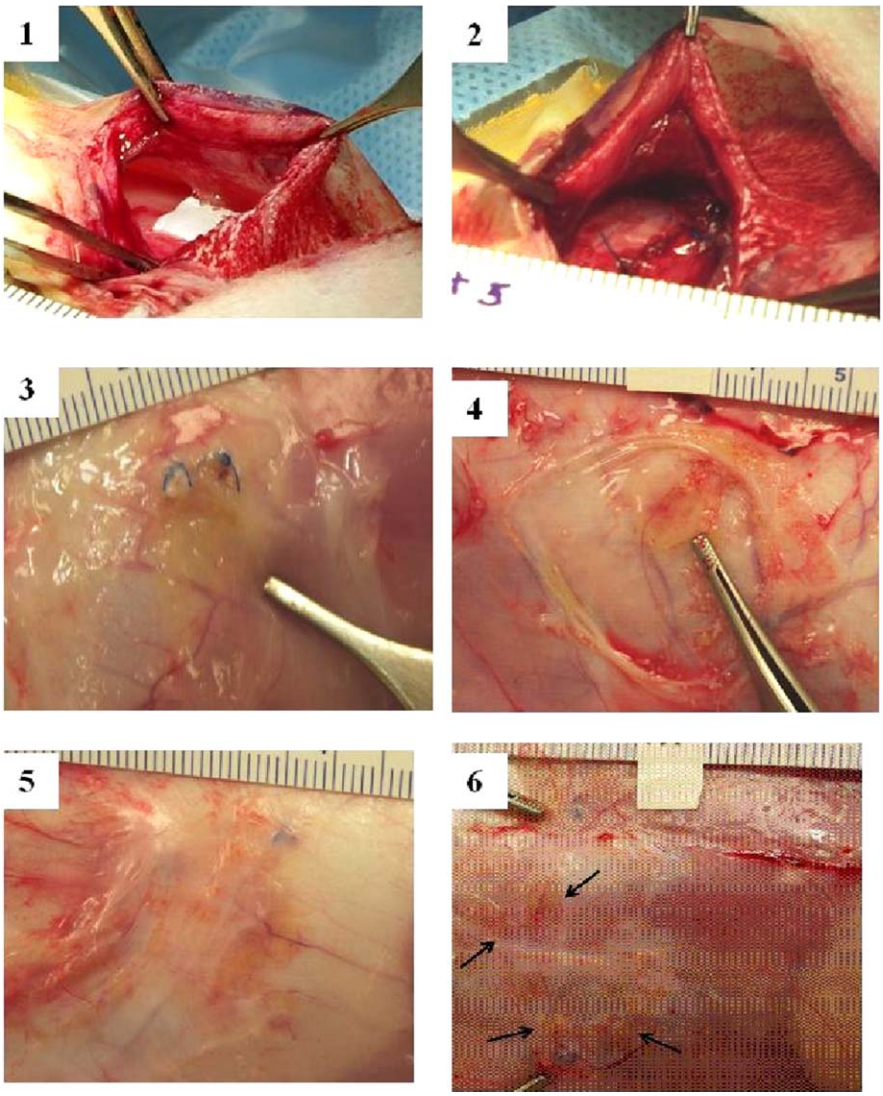

Figure 11. Representative surgery and necropsy images of TD55 sample: (1) cellulose implant after placement in position in subcutaneous pocket, (2) the implant was nearly indistinguishable from underlying tissue upon placement, (3) 2 weeks after implantation, (4) 4 weeks after implantation, (5) 12 weeks after implantation (the implant was severely degraded in both cases, and there was discoloration of the tissue; any implant remaining was very diffuse and thin, (6) 26 weeks after implantation (the implant was severely degraded and there was discoloration of the tissue; any implant remaining was very diffuse and thin. Stay sutures are visible, and arrows indicate diffuse small areas of discoloration that may indicate fragments of remaining TD55 implant material). [Color figure can be viewed in the online issue, which is available at wileyonlinelibrary.com.]

Table II. *In Vivo* Implant Degradation Scoring

	Degradation scoring			
Implants	2 weeks	4 weeks	12 weeks	26 weeks
CD1 (control) Crosslinked bovine collagen	0.25	0.75	3.5	4
CD2 (control) Microbial cellulose	0	0	0	1
TD55	2.5	2.5	3	3.25
TD84	2.5	2.75	2.75	3.25
TD50	2.5	2.5	3	3.25
TD94	2.75	2.75	3	3.5

Resorption Scoring: 0 = same as when implanted, 1 = slight fragmentation, 2 = moderate fragmentation, 3 = severe fragmentation, 4 = not able to score.

with pre-irradiated cellulose. Figure 9 compares results of the *in vitro* degradation extent at 14 days for both irradiated and non-irradiated OMCs, oxidized for various periods of time (1–4 hours). There is a considerable and comparable weight loss in both types of samples oxidized for 3 and 4 hours. However, degradation extent of the samples oxidized for 1 hour is significantly higher for pre-irradiated cellulose. Such a phenomenon further substantiates the hypothesis that pre-irradiated OMC samples consist of shorter and more efficiently oxidized glucan chains that are more easily and quickly hydrolyzed. In contrast, the nonirradiated OMCs consist of longer chains that may contain more randomly scattered dialdehyde groups. As degradation of OMCs proceeds the degree of polymerization decreases (Figure 10). After 7 days *in vitro* incubation in SBF the weight-average molecular weight of OMC decreased almost 2-fold in comparison with native cellulose (45,090 g/mol compared to 88,275 g/mol).

In Vivo Degradation Rate and Safety/Biocompatibility

The susceptibility of γ-irradiated, oxidized cellulose samples and controls to degradation *in vivo* was determined after subcutaneous implantation in the male New Zealand White Rabbit.

Necropsy Gross Observations

The control implants did not show any discoloration throughout the study. After 2 weeks, there was some gross red discoloration noted around all test material implants, with the least amount being around TD94. The discoloration increased slightly at all test material sites after four weeks, with the reddest discoloration being observed around TD94. At 12 weeks, red discoloration at all sites was similar to that observed at two weeks, with the least amount observed around TD94. No infection was observed at any time point. At 26 weeks, slight fibrosis was observed around all implants except the crosslinked bovine tendon collagen.

Gross vascularization (a sign of chronic inflammation) was also rarely observed at the early time points, but tended to increase at the 12- and 26-week time points, being greatest at the latter. It was most prominent around the TD55 implant and least prominent around the TD50 implant at 2 weeks. No gross vascularization was observed around the control implants at 2 and 4 weeks, but it was evident after 12 weeks, especially around the native microbial cellulose implant. The crosslinked bovine tendon collagen and all test material implant sites also showed some gross vascularization after 12 weeks. It was about equally present at all sites, except the crosslinked bovine tendon collagen sites, where it was not present at all at 26 weeks.

Representative surgery and necropsy images of test material TD55 are shown in Figure 11. The native microbial cellulose implant showed no sign of degradation over the entire period of study. Crosslinked bovine tendon collagen on the other hand, showed some degradation at 2 weeks, was significantly degraded at 4 weeks, and was essentially not present at 12 and 26 weeks. All of the test devices showed degradation at all time points (Table II), but interestingly, while they initially appeared to degrade quickly, they did not continue to degrade as rapidly. A similar behavior was observed for the OMC samples during an accelerated *in vitro* degradation study that showed a very rapid initial degradation of oxidized cellulose samples over the first 48 hours but leveling off of the rate at 72–96 hours (Figure 12). *In vivo* TD94 showed the most rapid degradation at 2 weeks (Table II) but at 4 weeks, degradation of TD94 and TD84 were similar, whereas TD 55 and TD50 showed slightly less degradation. At 12 weeks, degradation of all test devices was very similar. At 26 weeks, there were some remnants of all test devices still present (in the form of tissue discoloration), but the native microbial cellulose was unchanged.

Histological Observations

Representative histology images of test material TD55 and controls (CD1 and CD2) after 26 weeks postimplantation are shown in Figure 13. The inflammatory response to the implant materials was consistent with a foreign body response, characterized by variable numbers of macrophages, foreign body giant cells and with minimal to mild numbers (a score of 1–2) of neutrophils. Eosinophils were not uncommon and plasma cells were rarely seen. Fibrosis generally consisted of narrow to moderately thick bands, with the exception of the native microbial cellulose, which presented with increased fibrous capsule formation around the implants at 12 weeks.

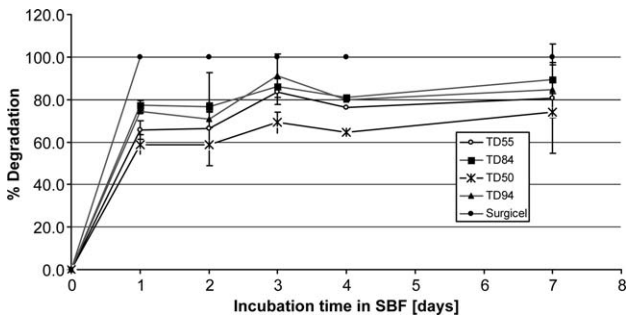

Figure 12. *In vitro* degradation profiles (37°C) for the OMC formulations used in the animal studies and Surgicel® (oxidized regenerated plant cellulose; Ethicon, Somerville, NJ) as control.

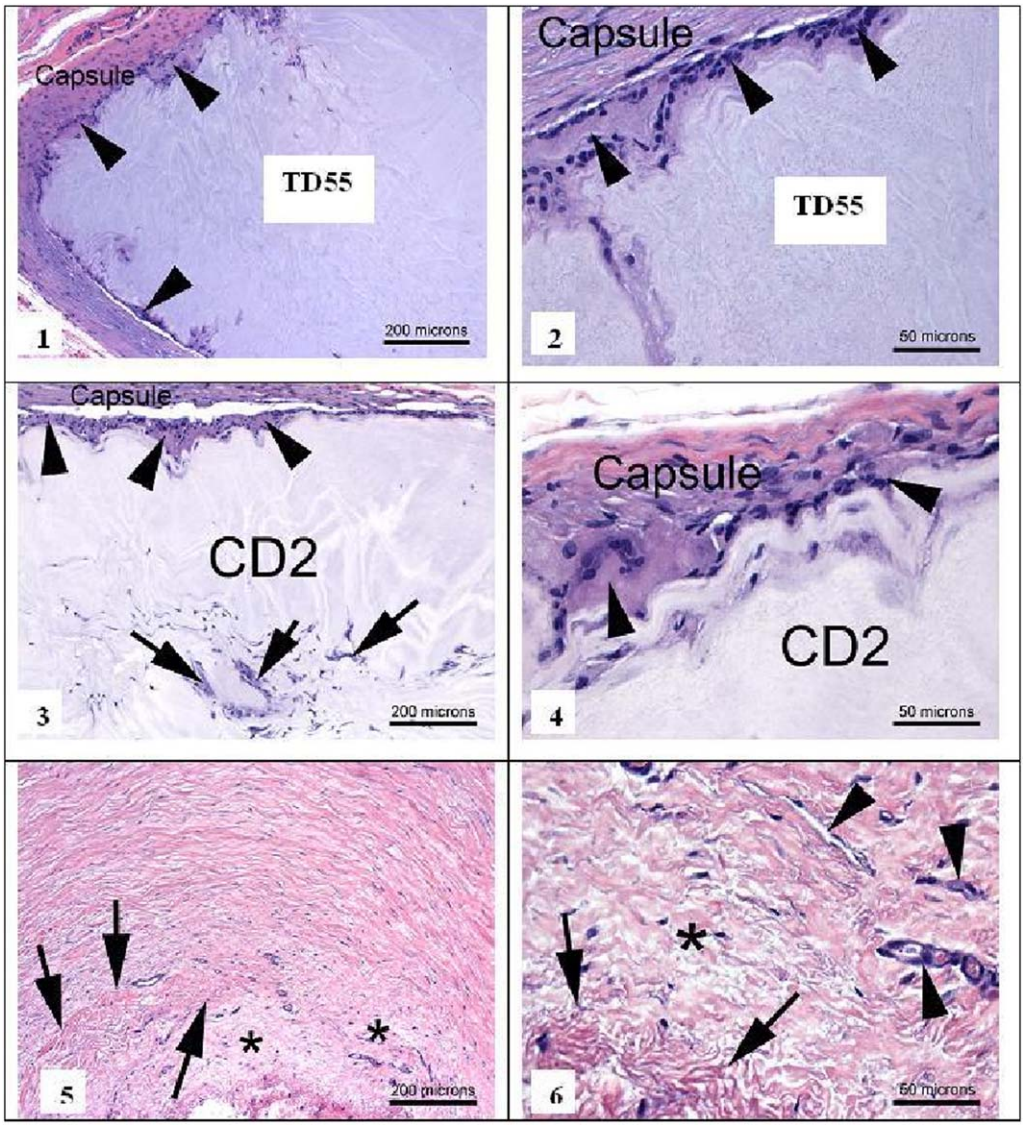

Figure 13. Representative histology images (H&E staining) of OMC sample-TD55 (1 and 2), microbial cellulose (control CD2) (3 and 4), and crosslinked bovine collagen (control CD1) (5 and 6) at 26 weeks postimplantation: (1 and 2) layer of foreign body giant cells (arrowheads) and scattered macrophages surrounding the remaining portion of OMC (TD55) with an evident capsule formation; (3 and 4) layer of foreign body giant cells (arrowheads) and macrophages surround native microbial cellulose (control CD2) —arrows point to foreign body giant cells and macrophages infiltrating control material; (5 and 6) this animal had no crosslinked bovine collagen (control CD1) remaining microscopically—asterisks indicate less mature fibrous tissue; arrows point to mature, pre-existing fibrous tissue; arrowheads point to the small, new vessels more frequently seen in the less mature tissue. [Color figure can be viewed in the online issue, which is available at wileyonlinelibrary.com.]

At the early time points (2, 4 weeks), the inflammatory reaction to TD94 was most prominent compared to the other test materials. This is consistent with a very rapidly absorbed material. At 12 and 26 weeks, macrophages and giant cell responses were noted for all the test materials, but the highest scores were seen with TD84, and to a lesser extent, TD50. This finding likely indicates that these materials were resorbing more slowly than the TD94 material.

Compared to the control implants all test materials were considered to be either nonirritants or slight irritants at 2, 12, or 26 weeks (Figures 14 and 15). At the 4-week time point only, TD55 and TD94 were considered to be moderate irritants when compared to the native microbial cellulose.

At 2 weeks, extracellular PAS staining of the implant material roughly correlated with the percentage of dialdehyde content (percent oxidation) in the test materials (data not shown). The correlation with oxidation level of the test materials did not hold up as well at subsequent time points, presumably because of dialdehyde loss as the materials degraded. There was some intracellular PAS staining within the cytoplasm of macrophages and foreign body giant cells, regardless of the type of material present, at all time points. This finding is not surprising as the PAS stain detects carbohydrates that are commonly present intracellularly. For the oxidized samples, intracellular PAS staining may also reflect uptake of test materials.

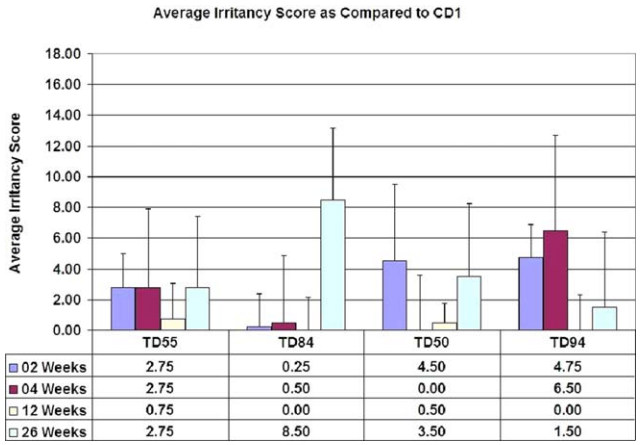

	TD55	TD84	TD50	TD94
02 Weeks	2.75	0.25	4.50	4.75
04 Weeks	2.75	0.50	0.00	6.50
12 Weeks	0.75	0.00	0.50	0.00
26 Weeks	2.75	8.50	3.50	1.50

Figure 14. The average irritancy score of the test materials compared to the crosslinked bovine tendon collagen. Nonirritant = (0.0–2.9); slight irritant = (3.0–8.9); moderate irritant = (9.0–15.0); severe irritant = (>15.0). [Color figure can be viewed in the online issue, which is available at wileyonlinelibrary.com.]

Potential Mechanism of *In Vivo* Resorption

Based on our results we suggest that the potential mechanism of OMC resorption consists of two steps: (1) initial rapid resorption *via* hydrolysis of oxidized domains resulting in degradation of about 70–80% and (2) formation of short oligosaccharides that are further cleared by phagocytosis, where the action of macrophages and giant cells break down the short glucan chains to the point where they can be engulfed by the cells.

This hypothesis is in line with the results of the study by Pierce et al., which showed that Surgicel®, a hemostat made from nitrogen dioxide oxidized regenerated plant cellulose, consists of two potentially biologically reactive components: (1) the readily soluble anhydroglucuronic acid that degrades via hydrolysis and is cleared within 18 hours and (2) fibrous residues requiring macrophage phagocytosis for subsequent clearance.[35] Also, the study by Dimitrijevich et al. suggested a similar mechanism for resorption of Interceed®, also an oxidized, regenerated plant cellulose adhesion barrier, in which the polymer undergoes chain-shortening to give oligomers, which in the presence of plasma or serum, are further hydrolyzed to smaller fragments.[36,37]

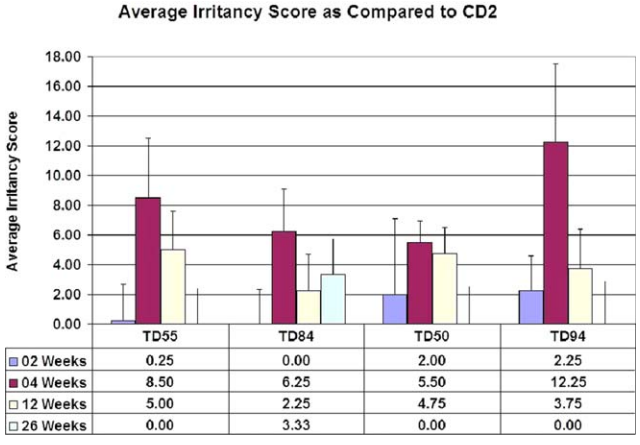

	TD55	TD84	TD50	TD94
02 Weeks	0.25	0.00	2.00	2.25
04 Weeks	8.50	6.25	5.50	12.25
12 Weeks	5.00	2.25	4.75	3.75
26 Weeks	0.00	3.33	0.00	0.00

Figure 15. The average irritancy score of the test materials compared to the native microbial cellulose. Nonirritant = (0.0–2.9); slight irritant = (3.0–8.9); moderate irritant = (9.0–15.0); severe irritant = (>15.0). [Color figure can be viewed in the online issue, which is available at wileyonlinelibrary.com.]

CONCLUSIONS

A highly conformable and mechanically stable biomaterial with potential for soft tissue repair can be produced from pre-γ-irradiated OMC. Surprisingly pre-irradiation with gamma radiation was a key to maintain conformability, rehydration capability, and strength in the oxidized materials. *In vivo* these oxidized materials showed degradation as early as 2 weeks but, interestingly, there continued to be some evidence of material present at time points out to 26 weeks. This is consistent with *in vitro* degradation where initial rapid degradation was followed by a slower degradation phase. The inflammatory reaction to OMC's was most prominent at the early time point, which is consistent with a rapidly degrading material. The four tested samples were considered to be either nonirritants or slight irritants, when compared to native microbial cellulose and crosslinked bovine tendon collagen. The potential mechanism of OMC resorption is proposed to consist of two steps: (1) an initial rapid hydrolytic degradation and resorption and (2) clearance of resultant short oligosaccharides by phagocytosis.

Here we show that a relatively simple, reproducible, and controlled chemical oxidation of pre-irradiated microbial cellulose sheets results in a resorbable and fully conformable membrane that can be rapidly rehydrated in aqueous fluids. This process provides access to a unique resorbable biomaterial that is biocompatible and may have properties clinically useful for soft tissue repair and other medical applications.

ACKNOWLEDGMENTS

We thank Peter Schaut for help with SEM and Amanda Marchese for help with XRD and FTIR testing. Thanks to H. Vince Mendenhall, DVM, PhD, and his team at Preclinical Surgical Services. Thanks to Joan R. Wicks, PhD, DVM, DACVP, Serge Rouselle, DVM, and the team at Alizee Pathology, LLC. Thanks to Christopher Flounders for help with graphs preparation.

REFERENCES

1. O'Sullivan, A. *Cellulose* **1997**, *4*, 173.
2. Fontana, J. D.; De Sousa, A. M.; Fontana, C. K.; Torriani, I. L.; Moreschi, J. C..; Gallotti, B. J.; deSouza, S. J.; Narcisco, G. P.; Bichara, J. H.; Farah, L. F. *Appl. Biochem. Biotechnol.* **1990**, *24/25*, 253.
3. Nishi, Y.; Uryu, M.; Yamanaka, S.; Watanabe, K.; Kitamura, N.; Iguchi, M.; Mitsuhashi, S. *J. Mater. Sci.* **1990**, *25*, 2997.
4. Shah, J.; Brown, R. M., Jr. *Appl. Microbiol. Biotechnol.* **2005**, *66*, 352.
5. Alvarez, O.; Patel, M.; Booker, J.; Markowitz, L. *Wounds* **2004**, *16*, 224.
6. Czaja, W.; Young, D.; Kawecki, M.; Brown, R. M., Jr. *Biomacromolecules* **2007**, *8*, 1.

7. Klemm, D.; Heublein, B.; Fink, H. P.; Bohn, A. *Angew. Chem. Int. Ed.* **2005**, *44*, 3358.
8. Bodin, A.; Concaro, S.; Brittberg, M.; Gatenholm, P. *J. Tissue Eng. Regen. Med.* **2007**, *1*, 406.
9. Svensson, A.; Nicklasson, E.; Harrah, T.; Panilaitis, B.; Kaplan, D. L.; Brittberg, M.; Gatenholm, P. *Biomaterials* **2005**, *26*, 419.
10. Yamada, Y.; Yukphan, P.; Thi Lan Vu, H.; Muramatsu, Y.; Ochaikul, D.; Tanasupawat, S.; Nakagawa, Y. *J. Gen. Appl. Microbiol.* **2012**, *58*, 397.
11. Stilwell, R.; Marks, M.; Saferstein, L.; Wiseman, D. In Handbook of Biodegradable Polymers; Domb, A. J., Kost, J., Wiseman, D. M., Eds.; HAP: Amsterdam, **1997**; p 291.
12. Nevell, T. In Methods in Carbohydrate Chemistry; Green, J. W., Bemiller, J. M., Eds.; Academic Press: New York, **1963**; Vol. *3*, p 164.
13. Kim, U.; Kuga, S.; Wada, M.; Okano, T.; Kondo, T. *Biomacromolecules* **2000**, *1*, 488.
14. Calvini, P.; Gorassini, A.; Luciano, G.; Franceschi, E. *Vib. Spectrosc.* **2006**, *40*, 177.
15. Singh, M.; Ray, A. R.; Vasudevan, P. *Biomaterials* **1982**, *3*, 16.
16. Devi, K.; Sinha, T. J. M.; Vasudevan, P. *Biomaterials* **1986**, *7*, 193.
17. Laurence, S.; Bareille, R.; Baquey, C.; Fricain, J. C. *J. Biomed. Mater. Res.* **2005**, *73A*, 422.
18. Roychowdhury, P.; Kumar, V. *J. Biomed. Mater. Res.* **2006**, *76A*, 300.
19. Li, J.; Wan, Y.; Li, L.; Liang, H.; Wang, J. *Mater. Sci. Eng. C* **2009**, *29*, 1635.
20. Yadav, V.; Paniliatis, J.; Shi, H.; Lee, K.; Cebe, P.; Kaplan, D. *Appl. Environ. Microbiol.* **2010**, *76*, 6257.
21. Hu, Y.; Catchmark, J. M. *Acta Biomater.* **2011**, *7*, 2835.
22. Pommerening, K.; Rein, H.; Bertram, D.; Müller, R. *Carbohydr. Res.* **1992**, *233*, 219.
23. Losquadro, W. D.; Tatum, S. A.; Allen, M. J.; Mann, K. A. *Arch. Facial Plast. Surg.* **2009**, *11*, 104.
24. Segal, L.; Creely, J. J.; Martin, A. E., Jr.; Conrad, C. M. *Text Res. J.* **1959**, *29*, 786.
25. Bacterial endotoxin testing (WuXi App Tec, Inc.). http://www.wuxiapptec.com/pdfs/D-Endotoxin-w.pdf (accessed May 24, 2013)
26. Kokubo, T.; Kushitani, H.; Sakka, S.; Kitsugi, T.; Yamamuro, T. *J. Biomed. Mater. Res.* **1990**, *24*, 721.
27. ISO 10993. 2007 Biological evaluation of medical devices. Part 6: Tests for local effects after implantation. http://www.iso.org (accessed May 24, 2013).
28. Vicini, S.; Princi, E.; Luciano, G.; Franceschi, E.; Pedemonte, E.; Oldak, D. *Thermochim. Acta* **2004**, *418*, 123.
29. Mares, T.; Arthur, J. C. *Polym. Lett.* **1969**, *7*, 419.
30. Kovalev, G. V.; Bugaenko, L. T. *High Energ. Chem.* **2003**, *37*, 209.
31. Ershov, B. G. *Russ. Chem. Rev.* **1998**, *67*, 315.
32. Driscoll, M.; Stipanovic, A.; Winter, W.; Cheng, K.; Manning, M.; Spiese, J.; Galloway, R.; Cleland, M. R. *Radiat. Phys. Chem.* **2009**, *78*, 539.
33. Kim, U.; Wada, M.; Kuga, S. *Carbohydr. Polym.* **2004**, *56*, 7.
34. Mester, L. *ACS* **1955**, *77*, 5452.
35. Pierce, A. M.; Wiebkin, O. W.; Wilson, D. F. *J. Oral Pathol.* **1984**, *13*, 661.
36. Dimitrijevich, S. D.; Tatarko, M.; Gracy, R. W.; Linsky, C. B.; Olsen, C. *Carbohydr. Res.* **1990**, *195*, 247.
37. Dimitrijevich, S. D.; Tatarko, M.; Gracy, R. W.; Wise, G. E.; Oakford, L. X.; Linsky, C. B.; Kamp, L. *Carbohydr. Res.* **1990**, *198*, 331.